15th IFK
Proc. of the 15th International Fluid Power Conference < Symposium/Conference >
< DOI >

# Optimal preliminary design of electro-mechanical actuators over drive-cycle for mobile machinery

Róger Mateus Sehnem, Samuel Kärnell and Liselott Ericson

*Linköping University, roger.mateus.sehnem@liu.se*

## Abstract.

Electromechanical actuators (EMAs) are increasingly being considered as replacements for hydraulic systems in mobile machinery due to electrification trends and efficiency requirements. Conventional EMA design approaches select representative steady-state operating points from the drive cycle, potentially yielding suboptimal designs when systems must operate over wide dynamic ranges. This paper explores the benefits of incorporating full drive-cycle dynamics into the preliminary design process using a bilevel optimization framework. A simplified hypothetical crane drive cycle demonstrates the approach by comparing dynamic optimization against the more conventional static multi-design-point optimization. Despite a higher computational cost per optimization round, the dynamic approach consistently outperformed the static approach, achieving not only copper losses that are four times lower than using the static optimization approach, but also smaller diameter, and superior trajectory tracking while respecting voltage and current limits. It is shown that the performance advantages persist when evaluated on drive cycles outside the optimized one. While the simplified models (neglecting iron losses, thermal limits, and saturation effects) limit direct applicability to real designs, the results demonstrate significant potential benefits of drive-cycle-aware optimization for preliminary EMA design in mobile machinery applications.

**Keywords.** Optimization, EMA, PMSM, Mobile machines, Optimal control.

## 1. Introduction

With the current global trend towards electrification and stricter regulations on emissions, mobile machinery is being pushed towards being electrically driven. Since current battery technology has lower power density than traditional fuel-driven solutions, the efficiency of the actuators is now becoming a much more relevant design goal. This is one of the reasons why electromechanical actuators (EMAs) are now being considered as, to some extent, replacements for hydraulics in mobile machinery.

Designing an EMA can be framed as a complex optimization problem that needs to consider several physical domains. Optimality in this context can often be framed as maximizing the power density of the actuator and its efficiency while ensuring that the relevant constraints are met or not exceeded, e.g., maximum current and desired power. Most systems in engineering can be precisely described by nonlinear differential equations. Dealing with differential equations in preliminary design is, however, difficult, and it is a common practice to simplify the design process by considering only static or steady-state behavior. To this end, the designer needs to choose a design point that is representative of the system's operation range. In cases where the system operates in a wide range of conditions, as in EMAs for mobile machinery, this choice is by no means trivial, and this approach can lead to suboptimal designs.

In reality, the designer is either attempting to optimize the performance of the system over the entire drive cycle on which the EMA will operate or a significant reference drive cycle exemplified for a lorry crane application in [1]. In any case, for drive cycles that require significant transient behavior of the system, it is reasonable to expect that considering the full dynamics of the system can lead to better designs than using steady state approaches. The main goal of this paper is to show that this is indeed the case.

### 1.1. *Previous Work*

Considering more of the drive cycle in design has been proposed by several authors in different ways. For instance, [2] proposed a convex model fitted on high-fidelity simulation data to allow efficient convex optimization and global optimum results. The approach considers a simplified dynamical model, thus attempting to be more representative of the system behavior. Another approach is to somehow aggregate several different steady state operating points into some that are then used to design the electrical machine, this is the approach of [3], where the energy center of gravity (ECG) of the torque-speed plot is used to create 8 clusters, which are then weighted according to their energy usage in the drive cycle and then have their centers used as steady state design points. Another example of this approach is [4], which uses a multi-objective optimization approach to optimize the design of a PMSM considering multiple operating points and uses simple formulas to estimate the transient losses in the optimization problem. However, all those methods have strong simplifying assumptions about the true dynamics of the system.

The main challenge in the attempt to consider the full dynamics of the system in the design process is that the output of the system depends on the control input, and if one chooses a suboptimal control strategy, the performance of the system will be underestimated. The problem of finding an optimal control strategy for a given system is known as an optimal control problem (OCP), which is known to be numerically difficult to solve in the nonlinear case [5, 6]. Considering the optimization of the system parameters together with the control inputs is thus expected to be an even more sensitive and hard problem.

However, when one considers linear systems with quadratic cost functionals in the state deviations and control inputs, known as the Linear Quadratic Regulator (LQR) problem [5, 6], the problem has an analytical solution. Although the LQR problem is designed for linear systems, it can be used to design controllers for nonlinear systems with the usage of some form of linearization technique, giving a controller that in practice works well for a wide range of operating conditions in many applications.

### 1.2. *Contribution*

To address the conjoint optimization of an EMA and the solution of the OCP in a sensible way, in this work, a two-step optimization process is used. The lower problem is a standard OCP, which, for a given system, finds the optimal control inputs that minimize a relevant cost functional. The upper problem then chooses the system parameters to minimize a cost function that penalizes energy loss, tracking error and the size of the EMA, which is evaluated by solving the lower OCP. Dividing the optimization as described is known as bilevel optimization and has been used in several applications [7]. In this way, it is possible to directly consider the full dynamics of the system in the design process. To simplify the OCP problem, a standard field-oriented control with feedback linearization and P controllers for the currents and velocity and a PI controller for the position are used. The controller gains are chosen using the LQR method on an error system, allowing the efficient solution of the internal OCP for a given set of system parameters.

As a proof of concept, this paper explores the potential benefits of considering the full dynamics of the system in the preliminary design of an EMA for a simplified hypothetical loader crane drive cycle. A standard PMSM model from [8] with parameters calculated from physical dimensions is considered, together with very simple models for the gears and ball screw. The approach is then compared to using only some relevant design points considering only the steady-state dynamics of the system, analogous to the approach of [4]. The PMSM model used in this work neglects several effects that are present in real machines, such as saturation, thermal limits, eddy currents, hysteresis losses and non-sinusoidal magnetic field distributions. The same can be said about the mechanical components, their models are overly simplified to be useful in the design of a real EMA. However, the models are considered to be sufficient for the purpose of this work, which is to explore the potential benefits of considering the full dynamics of the system in the design of an EMA for a hypothetical drive cycle.

The results show that the EMA optimized considering the full system dynamics dissipates four times less energy to follow the design trajectory, all while being able to respect the electrical constraints and having the desired geometry.

## 2. Electro-mechanical Actuator Model

The EMA model consists of a PMSM, a gearbox and a ball screw and is shown schematically in Figure 2.1. In the following subsections, the model of each component is described in detail.

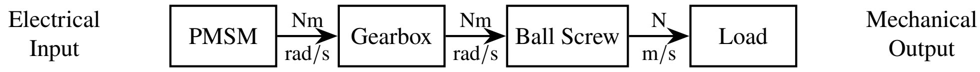


Figure 2.1 Schematic representation of the EMA system considered. The PMSM drives a ball screw through a gearbox, which then moves a load linearly. The electrical subsystem is represented on the left, while the mechanical subsystem is represented on the right. The arrows indicate the power flows in the system.

### 2.1. *Permanent Magnet Synchronous Machine*

The PMSM model is traditionally composed of electro-mechanical constants that are usually obtained from experimental data or finite element analysis. In this work, however, the PMSM parameters are estimated from simplified physical considerations of the motor geometry and magnetic field distribution. This not only allows a more direct connection between the physical dimensions of the motor and its performance but also has very low computational complexity. The model follows the developments in [8] closely, with the additional parametrization for the torque constant $K_m$ and stator resistance $R_S$ from physical dimensions, which are not directly given in the reference. The PMSM model assumes a sinusoidal magnetic field distribution, no saturation, eddy current or hysteresis losses and is given by the following set of differential equations in the stator reference frame [8]:

$$\begin{aligned}
\frac{d\theta_r}{dt} &= \omega, \\
J\frac{d\omega}{dt} &= K_m\left(-i_{Sa}\sin(n_p\theta_r) + i_{Sb}\cos(n_p\theta_r)\right) - f(\omega) - \tau_L, \\
L_S\frac{di_{Sa}}{dt} &= -R_S i_{Sa} + K_m\sin(n_p\theta_r)\omega + u_{Sa}, \\
L_S\frac{di_{Sb}}{dt} &= -R_S i_{Sb} - K_m\cos(n_p\theta_r)\omega + u_{Sb}.
\end{aligned} \tag{2.1}$$

where $\theta_r$ is the rotor position, $\omega$ is the rotor angular velocity, $i_{Sa}$ and $i_{Sb}$ are the stator currents in phases a and b, $u_{Sa}$ and $u_{Sb}$ are the stator voltages in phases a and b, $J$ is the rotor inertia,

$K_m$ is the motor torque constant, $n_p$ is the number of pole pairs. $L_S$ is the stator inductance, $R_S$ is the stator resistance, $f(\omega)$ is a friction model and $\tau_L$ is the load torque.

The derivation of $L_S$ closely follows the developments in [8]. Both $L_S$ and $K_m$ assume a full-pinched winding, but the model can be adapted to short-pinched or long-pinched windings by adding the winding factor $\kappa_w$ to the equations for $L_S$ and $K_m$.

### 2.1.1. *Stator Inductance from Physical Dimensions*

For the parameters calculation, assume that the magnetic field distribution in the air gap is approximated by a sinusoidal distribution for each phase. Following [8], the total magnetic field in the air gap due to the stator currents is then given by

$$\boldsymbol{B}_s(i_{Sa}, i_{Sb}, r, \theta) = \boldsymbol{B}_{Sa} + \boldsymbol{B}_{Sb} = \frac{\mu_0 N_s r_r}{2g}\frac{1}{r}\left(i_{Sa} cos(\theta) + i_{Sb}\sin(\theta)\right)\boldsymbol{e}_r, \tag{2.2}$$

where $\mu_0$ is the permeability of free space, $N_s$ is the number of turns per phase, $r_r$ is the rotor radius, $g$ is the air gap length, $r$ is the radial position in the air gap, $\theta$ is the angular position in the air gap, and $\boldsymbol{e}_r$ is the radial unit vector. The magnets in the rotor of the PMSM are distributed such that the magnetic field in the air gap generated by the rotor is also sinusoidal, thus

$$\boldsymbol{B}_R = B_m \frac{r_r}{r}\cos(\theta - \theta_r)\boldsymbol{e}_r, \tag{2.3}$$

where $B_m$ is the peak magnetic field in the air gap generated by the rotor.

The total flux linkage of the stator describes how much magnetic flux flows through the stator windings and is a useful quantity to calculate $K_m$ and $L_S$. It is defined as

$$\lambda_{Sa}(\boldsymbol{i}_s, \theta_R) = {}_s\lambda_{Sa}(\boldsymbol{i}_s, \theta_r) + {}_r\lambda_{Sa}(\theta_r) = \int_{\mathbb{L}_{Sa}} \boldsymbol{B}_s d\boldsymbol{S} + \int_{\mathbb{L}_{Sa}} \boldsymbol{B}_R d\boldsymbol{S}, \tag{2.4}$$

where $\boldsymbol{i}_s = \begin{bmatrix} i_{Sa} & i_{Sb} \end{bmatrix}^T$ and $\mathbb{L}_{Sa}$ is a set of surfaces that envelops all stator windings of phase $a$. To calculate ${}_s\lambda_{Sa}$, one calculates the flux in a single loop of the stator and then integrates over all loops. If the given loop is at an angle $\theta$ from the $a$ phase of the stator, then its other side is, considering full-pinched windings, at $\theta - \pi$. Thus, the flux in the cylindrical surface is given, for the $a$ phase of the stator, by

$${}_s\phi_{Sa}(\boldsymbol{i}_s, \theta) = \int_{\theta-\pi}^{\theta}\int_0^{l_1} \boldsymbol{B}_S(\boldsymbol{i}_s, \theta)|_{r_s} \boldsymbol{e_r} \cdot (r_s d\theta dz \boldsymbol{e_r}) = \frac{\mu_0 r_r l_1 N_s}{g}\left(i_{Sa}\sin(\theta) - i_{Sb}\cos(\theta)\right). \tag{2.5}$$

The flux linkage ${}_s\lambda_S$ between $\theta$ and $\theta + d\theta$ is then given by multiplying by turns density distribution, as

$$d\,{}_s\lambda_{Sa} = {}_s\phi_{Sa}(\boldsymbol{i}_s, r, \theta)\frac{N_s}{2}\sin(\theta)d\theta = \frac{\mu_0 r_r l_1 N_s}{g}\left(i_{Sa}\sin(\theta) - i_{Sb}\cos(\theta)\right)\frac{N_s}{2}\sin(\theta)d\theta, \tag{2.6}$$

where the $\frac{N_s}{2}\sin(\theta)$ term comes from the winding distribution in the stator. Integrating Equation (2.6) from 0 to $\pi$ gives the total flux linkage in phase $a$ of the stator due to the stator magnetic field, which is given by

$${}_s\lambda_{Sa}(\boldsymbol{i}_s) = \frac{\mu_0 r_r l_1 \pi N_s^2}{4g} i_{Sa} = \frac{\mu_0 l_1 l_2 \pi N_s^2}{8g} i_{Sa} \coloneqq L_S i_{Sa}, \tag{2.7}$$

where $l_2 = 2r_r$ is the stator diameter. Equation (2.7) defines the stator inductance $L_S$. The flux linkage in phase $b$ of the stator can be calculated in a similar way, giving the same result for $L_S$.

### 2.1.2. *Torque Constant from Physical Dimensions*

To get the rotor flux linkage, it is important to account for the leakage $\kappa$ in the magnetic field. Following [8], the rotor flux linkage at the stator side is given by modifying Equation (2.3) to

$$\boldsymbol{B}_R|_{r_s} = \kappa B_m \frac{r_r}{r_s} \cos(\theta - \theta_r)\boldsymbol{e}_r, \tag{2.8}$$

where $r_s$ is the stator radius.

To calculate ${}_r\lambda_{Sa}$, the same approach as in the stator flux linkage is used. The flux in a single loop of the stator at angle $\theta$ is given by

$${}_r\phi_{Ra} = \int_{\theta-\pi}^{\theta} \int_0^{l_1} \kappa B_m \frac{r_r}{r_s} \cos(\theta - \theta_r) r_s dr dz = 2\kappa B_m l_1 r_r \sin(\theta - \theta_r). \tag{2.9}$$

With that is possible to write the rotor flux linkage differential, using the sinusoidal winding for the stator phase $a$, as

$$d\,{}_r\lambda_{Sa} = \phi_{Ra} \frac{N_S}{2} sin(\theta) d\theta = \kappa B_m l_1 r_r N_S \sin(\theta - \theta_r) sin(\theta) d\theta. \tag{2.10}$$

Integrating Equation (2.10) from 0 to $\pi$ gives

$${}_r\lambda_{Sa} = \int_0^{\pi} \kappa B_m l_1 r_r N_S \sin(\theta - \theta_r) sin(\theta) d\theta = \kappa B_m l_1 r_r N_S \frac{\pi}{2} \cos(\theta_r) \coloneqq K_m \cos(\theta_r), \tag{2.11}$$

which defines the torque constant $K_m$.

### 2.1.3. *Stator Resistance from Physical Dimensions*

The stator resistance is greatly defined by the length of the wire used in the winding, which greatly depends on how it is wound. Figure 2.2 shows how one loop is wound in the stator.

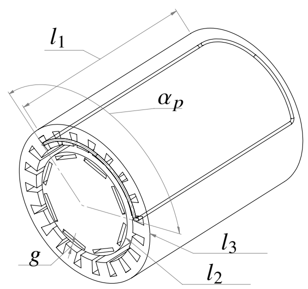


Figure 2.2 3D view of the PMSM with the stator and rotor, showing the stator length $l_1$, stator outer diameter $l_3$, stator inner diameter $l_2$, air gap $g$ and winding with pitch angle $\alpha_p$.

Figure 2.2 shows a single loop of winding. This winding is made with a wire of diameter $\phi_w$, and it is of a distributed winding type with pitch angle $\alpha_p$. Assuming no skin and proximity effects, the resistance $R_S$ of the stator winding can be estimated from the total length $l_s$ of wire used in the stator, its cross section $S_s$ and the electrical resistivity of the wire $\rho_{e,w}$ using

$$R_S = \frac{\rho_{e,w} l_s}{S_s}. \tag{2.12}$$

In a distributed winding stator, the total length of wire $l_s$ is given by the arc made by the angle $\alpha_p$, which is assumed to be at the stator's inner diameter $l_3$, together with the length of wire needed to traverse the stator's length $l_1$. Thus, the total length of wire is given by

$$l_s = (l_3\alpha_p + 2l_1)N_S n_p n_f, \tag{2.13}$$

where $n_f$ is the number of phases, $l_3$ is given by

$$l_3 = l_2 + 2g. \tag{2.14}$$

Thus, the resistance of the stator winding is fully defined by the physical dimensions of the motor as

$$R_S = \frac{(l_3\alpha_p + 2l_1)N_S n_p n_f \rho_{e,w}}{S_s}. \tag{2.15}$$

### 2.2. *Gearbox and Ball Screw*

The gearbox and ball screw mechanisms are modeled in a very simplified way, assuming a constant efficiency $\eta_g$ and $\eta_{bs}$ for the gearbox and ball screw, respectively. Each of the mechanisms is modeled as a simple torque and speed transformation, given by

$$\begin{aligned} \tau_{out} &= \eta_g G \tau_{in}, \\ \omega_{out} &= \frac{\omega_{in}}{G}, \end{aligned} \tag{2.16}$$

for the gearbox, where $G$ is the gear ratio, $\tau_{in}$ and $\omega_{in}$ are the input torque and speed, respectively, and $\tau_{out}$ and $\omega_{out}$ are the output torque and speed, respectively. The ball screw is modeled in a similar way, given by

$$\begin{aligned} F_{out} &= \eta_{bs} \frac{2\pi}{p} \tau_{in}, \\ v_{out} &= \frac{p}{2\pi} \omega_{in}, \end{aligned} \tag{2.17}$$

where $p$ is the pitch of the ball screw, $\tau_{in}$ and $\omega_{in}$ are the input torque and speed, respectively, and $F_{out}$ and $v_{out}$ are the output force and speed, respectively.

## 3. Controller

To be able to evaluate the performance of the EMA over the drive cycle, a control strategy that allows the EMA to follow the desired trajectory needs to be defined. This can be achieved by following [8] and using a standard field-oriented control with feedback linearization, P controllers for the currents and velocity and a PI controller for the position. The controller gains are in turn chosen using the LQR method, allowing the efficient computation of the optimal controller gains for a given set of system parameters.

### 3.1. *Field-oriented Control*

The field-oriented control (FOC) is a widely used control strategy for PMSMs, which allows decoupling of the torque and flux control. The FOC is based on the transformation of the stator currents and voltages from the stationary reference frame to the rotating reference frame, which is aligned with the rotor magnetic field, known as the d-q reference frame.

To transform Equation (2.1) to the d-q reference frame, one simply rotates the stator currents and voltages by the electrical angle $n_p\theta$ using the counter-clockwise rotation matrix [8]. Applying the transformation to the PMSM model given by Equation (2.1), resulting in the following equations in the d-q reference frame

$$
\begin{aligned}
L_S \frac{di_d}{dt} &= -R_S i_d + n_p L_S \omega i_q + u_d, \\
L_S \frac{di_q}{dt} &= -R_S i_q - n_p L_S \omega i_d - K_m \omega + u_q, \\
J \frac{d\omega}{dt} &= K_m i_q - f(\omega) - \tau_L, \\
\frac{d\theta}{dt} &= \omega,
\end{aligned} \tag{3.1}
$$

where $i_d$ and $i_q$ are the d-axis and q-axis stator currents, respectively, and $u_d$ and $u_q$ are the d-axis and q-axis stator voltages, respectively.

For a given reference trajectory $r(t) = \begin{bmatrix}\theta_{\text{ref}}(t) & \omega_{\text{ref}}(t) & \alpha_{\text{ref}}(t)\end{bmatrix}^T$, it is possible to calculate the reference state and control inputs trajectories needed to follow the reference trajectory. By considering its steady-state condition, it is possible to obtain the $i_{d,\text{ref}}$ that maximizes the torque, which in turn allows the obtention of $i_{q,\text{ref}}$ from $\omega_{\text{ref}}$ and $\alpha_{\text{ref}}$. With those, the reference voltages needed to follow the $r(t)$ directly follow.

With the reference system dynamics and control inputs, it is possible to create error dynamics by subtracting the reference dynamics from the system dynamics in Equation (3.1). This results in a nonlinear system that can be linearized using the following feedback linearization [8]

$$
\begin{aligned}
u_d &= -n_p L_S \omega i_q + u_{d,\text{ref}} + n_p L_S \omega_{\text{ref}} i_{q,\text{ref}} - L_S v_d, \\
u_q &= n_p L_S \omega i_d + u_{q,\text{ref}} - n_p L_S \omega_{\text{ref}} i_{d,\text{ref}} - L_S v_q,
\end{aligned} \tag{3.2}
$$

where $v_d$ and $v_q$ are the new control inputs for the error dynamics and the variables with subscript *ref* are the reference values. Using Equations (3.2) in the error dynamics results in a linear system that is amenable to standard linear control techniques.

To eliminate the steady-state error, an integrator state for the position error is introduced, $e_z = \int e_\theta dt$, which gives the augmented error state vector $\boldsymbol{e} = \begin{bmatrix} e_{i_d} & e_{i_q} & e_\omega & e_\theta & e_z \end{bmatrix}^T$. The augmented error dynamics is then given by

$$
\frac{d\boldsymbol{e}}{dt} = \begin{bmatrix}
-\frac{R_S}{L_S} & 0 & 0 & 0 & 0 \\
0 & -\frac{R_S}{L_S} & -\frac{K_m}{L_S} & 0 & 0 \\
0 & \frac{K_m}{J} & -\frac{f'(\omega)}{J} & 0 & 0 \\
0 & 0 & 1 & 0 & 0 \\
0 & 0 & 0 & 1 & 0
\end{bmatrix} \boldsymbol{e} + \begin{bmatrix}
\frac{1}{L_S} & 0 \\
0 & \frac{1}{L_S} \\
0 & 0 \\
0 & 0 \\
0 & 0
\end{bmatrix} \boldsymbol{v}, \tag{3.3}
$$

where $\boldsymbol{v} = \begin{bmatrix} v_d & v_q \end{bmatrix}^T$, for which a state feedback controller can be designed using the LQR method.

## 3.2. *Linear Quadratic Regulator Controller Design*

The setup of the LQR problem consists of finding the control input $\boldsymbol{u}(t)$ that minimizes the quadratic cost functional

$$
J = \int_0^\infty \left( \boldsymbol{e}(t)^T Q \boldsymbol{e}(t) + \boldsymbol{u}(t)^T R \boldsymbol{u}(t) \right) dt, \tag{3.4}
$$

where $Q$ is a positive semi-definite matrix and $R$ is a positive definite matrix. For a system given by

$$
\frac{d\boldsymbol{x}}{dt} = A\boldsymbol{x}(t) + B\boldsymbol{u}(t), \tag{3.5}
$$

the LQR problem consists of finding the control input $\boldsymbol{u}(t)$ that minimizes the cost functional of Equation (3.4), subject to the system dynamics of Equation (3.5).

This optimal control problem (OCP), for the linear systems, has an analytical solution given by the state feedback law, that is, a function $\boldsymbol{u}(x(t))$ that minimizes the cost functional of Equation (3.4), given by

$$\boldsymbol{u}(t) = -R^{-1}B^T S(t)x(t), \tag{3.6}$$

where $S$ is the solution of the matrix Riccati equation. To simplify the notation, the Kalman gain matrix is defined as

$$K(t) = R^{-1}B^T S(t). \tag{3.7}$$

Since the matrix $K(t)$ saturates to a constant matrix $K$ as $t \longrightarrow \infty$ [6], it is then possible to use what is known as the suboptimal control law, given by

$$\boldsymbol{u}(t) = -K(\infty)x(t). \tag{3.8}$$

To calculate the Kalman gain matrix $K(\infty)$, one solves the algebraic Riccati equation, given by

$$0 = A^T S + SA - SBR^{-1}B^T S + Q, \tag{3.9}$$

yielding the steady-state solution $S(\infty)$, which can be used to calculate the steady-state Kalman gain matrix $K(\infty)$ using Equation (3.7).

### 3.3. *Controller Summary*

By defining state and an input penalizing matrices $Q$ and $R$, it is possible to calculate the optimal state feedback gain matrix $K(\infty)$ by simply solving the algebraic Riccati Equation (3.9). This can be done using standard numerical methods optimized for this task and available in scientific computing libraries in Python [9], turning the lower level problem of finding the controller gains into a computationally efficient task.

The advantages of using the LQR method in this context are that solving the OCP is computationally efficient and that the resulting controller has good robustness properties [6], which is important since the same decision matrices $Q$ and $R$ are used for all the different EMA design attempts made by the optimizer.

It is important to note that the controller itself is based on a linearized model of the EMA, thus, it is not necessarily optimal for the nonlinear system. However, it is a good starting point and it is also representative of the controllers used in practice.

## 4. Optimization Problem Formulation

With the model and controller defined, the optimization problem can be formulated. The goal of the optimization problem is to find the design variables that minimize the cost function, while satisfying the constraints. The design variables are the physical dimensions of the EMA, which in turn define the parameters of the model. In the next subsections, the cost function of the upper problem is motivated and defined, the constraints are defined and the design variables are presented.

### 4.1. *Cost Function*

To examine the usefulness of considering the whole drive cycle in the optimization problem, the optimization of an EMA for a crane application is considered. This kind of application is nowadays dominated by hydraulic actuators, which have a high power density and are able to deliver high forces. To compete with hydraulic actuators, the designed EMA needs to have similar characteristics. There are, however, some differences between the two technologies that can be more easily accommodated in a crane application. One of those differences is related to the power density, it is probably much easier to accommodate a higher length than a larger diameter, thus, the power density might not be as critical as the diameter power density. This is one of the considerations made in the cost function, instead of trying to minimize the volume of the EMA, we try to minimize its diameter. Moreover, whatever the designed EMA is, it should be able to closely follow the desired load trajectory while respecting the constraints, the major ones being the maximum voltage and current that can be supplied to the EMA's motor.

One of the major motivators of substituting hydraulic actuators with EMAs is the potential increase in system efficiency. Thus, the cost function should also consider the efficiency of the EMA over the drive cycle. This is done by considering the total dissipated energy, which should be minimized. An important technical aspect to consider is that the optimizer might suggest designs that are not able to follow the desired trajectory and or are unstable. Those designs should be penalized in the cost function to prevent the optimizer from suggesting EMAs that are close to those designs, and thus, wasting computational resources evaluating those designs. This is done by penalizing the cost function with the squared residuals $\boldsymbol{r}(t)$ of the solver used to simulate the EMA dynamics over the drive cycle.

The above considerations motivate the following cost function for the dynamic optimization problem

$$J_{\text{dyn}}(\boldsymbol{x}(t)) = w_1 \int_0^T \frac{e_\theta(t)^2}{\max(|\theta_{\text{ref}}(t)|)} dt + w_2 l_2 + w_3 \frac{1}{E_{\text{ref}}} \int_0^T P_{\text{loss}}(t) dt + w_4 \int_0^T \|\boldsymbol{r}(t)\|^2 dt, \tag{4.1}$$

where the first term penalizes the position tracking error, the second term penalizes the diameter of the EMA, the third term penalizes the total energy loss over the drive cycle, and the fourth term penalizes the residuals of the EMA dynamics. The weights $w_1$, $w_2$, $w_3$ and $w_4$ are used to balance the different terms in the cost function, and $E_{\text{ref}}$ is given by

$$E_{\text{ref}} = \int_0^T |F_{\text{ref}}(t) v_{\text{ref}}(t)| dt. \tag{4.2}$$

The other normalization terms in Equation (4.1) are used to make the different terms in the cost function have similar magnitudes.

For the static optimization approach, the cost function is similar to Equation (4.1), but instead of integrating over the entire drive cycle, only a few significant design points are considered in the drive cycle. Thus, the cost function for the static approach is given by

$$J_{\text{stat}}(\boldsymbol{x}) = w_2 l_2 + w_3 \frac{1}{E_{\text{ref}}} \sum_{k=1}^{N_{dp}} P_{\text{loss},k} \Delta t_k \tag{4.3}$$

where $N_{dp}$ is the number of design points considered, $\Delta t_k$ is the time spent at design point $k$, $P_{\text{loss},k}$ is the power loss at design point $k$.

## 4.2. *Constraints*

One of the main constraints in designing an EMA is the maximum voltage and current that can be supplied to its motor. In real applications, another important constraint is the thermal limits of the motor, which are usually the limiting factor in the motor's power density. However, the main focus of this work is to show the potential of considering the entire drive cycle in the optimization problem, and thus, it suffices to consider only the electrical constraints, given by

$$\begin{aligned} u_{\text{mag}}(t) &= \sqrt{u_d(t)^2 + u_q(t)^2} \leq u_{\max}, \\ i_{\text{mag}}(t) &= \sqrt{i_d(t)^2 + i_q(t)^2} \leq i_{\max}, \end{aligned} \tag{4.4}$$

where $u_{\max}$ and $i_{\max}$ are the maximum voltage and current magnitude that can be supplied to the motor, respectively.

The constraints of Equation (4.4) need to be satisfied at each time instant. To enforce those constraints in the dynamic optimization approach, the penalty method is used, adding the following penalty terms to the cost function

$$G_{\text{dyn}}(\boldsymbol{x}(t)) = w_5 \max\left(0, \max(u_{\text{mag}}(t)) - u_{\max}\right)^2 + w_5 \max\left(0, \max(i_{\text{mag}}(t)) - i_{\max}\right)^2, \quad (4.5)$$

where $w_5$ is the penalty weight.

The static approach needs to consider the constraints of Equation (4.4) at each design point $k$, but to account for the steady-state dynamics, there is an additional constraint that needs to be satisfied, the residual of the steady-state dynamics $\boldsymbol{r}_k$, that is, the right hand side of Equation (3.1) with the derivatives zeroed out and evaluated at design point $k$. Since the steady-state, optimization-driven design needs to satisfy a set of constraints at every operating point, the problem is much more sensitive, and it was therefore also necessary to penalize non-integer values of the number of pole pairs $n_p$ and the number of turns per phase $N_S$. The constraints are enforced, in a similar way as in the dynamic case, that is, by adding the following penalty terms to the cost function

$$G_{\text{stat}}(\boldsymbol{x}) = w_6 \sum_{k=1}^{N_{dp}} \sin(\pi n_p)^2 + \sin(\pi N_S)^2 + w_7 \sum_{k=1}^{N_{dp}} \boldsymbol{r}_k^T \boldsymbol{r}_k + G_{\text{dyn}}(\boldsymbol{x}_k), \quad (4.6)$$

## 4.3. *Design Variables*

The design variables are the physical dimensions of the EMA, which in turn define the parameters of the model. The design variables are given, together with their respective bounds, in Table 4.1.

Table 4.1 Design variables and their respective lower and upper bounds, $\boldsymbol{l_b}$ and $\boldsymbol{u_b}$, respectively.

| Design variable | Description | | $\boldsymbol{l_b}$ | $\boldsymbol{u_b}$ | Dynamic | Static |
|---|---|---|---|---|---|---|
| $n_p$ | Number of pole pairs | | 1 | 6 | Yes | Yes |
| $l_2$ | Stator diameter | [m] | 0.01 | 0.3 | Yes | Yes |
| $l_1$ | Stator length | [m] | 0.1 | 1 | Yes | Yes |
| $N_S$ | Number of turns per phase | | 1 | 40 | Yes | Yes |
| $g$ | Air gap | [m] | 0.001 | 0.01 | Yes | Yes |
| $\alpha$ | Winding angle | [rad] | $\frac{\pi}{20}$ | $\pi$ | Yes | Yes |
| $g_{r_1}$ | First gear ratio | | 1 | 6 | Yes | Yes |
| $g_{r_2}$ | Second gear ratio | | 1 | 6 | Yes | Yes |
| $p$ | Ball screw pitch | [m] | 0.01 | 1 | Yes | Yes |
| $u_{q_k}$ | Voltage at design point $k$[V] | | $-u_{\max}$ | $u_{\max}$ | No | Yes |
| $i_{q_k}$ | Current at design point $k$[A] | | $-i_{\max}$ | $i_{\max}$ | No | Yes |

The chosen design variables allow one to fully define the EMA model, at least in the simplified form presented in this work. One should note that the design variables in the static approach include the voltages and currents at the design points, since those are needed to satisfy the steady-state dynamics at those points.

## 4.4. *Overview and Setup*

The dynamic and static optimization approaches were presented, an overview of how they were implemented is shown in Figure 4.1.

Both the static and dynamical optimization approaches were implemented using the same optimizer, Scipy's Differential Evolution [10], based on [11, 12]. A population size of 14 individuals was used, with a maximum of 1000 generations. The chosen weights are given in Table 4.2.

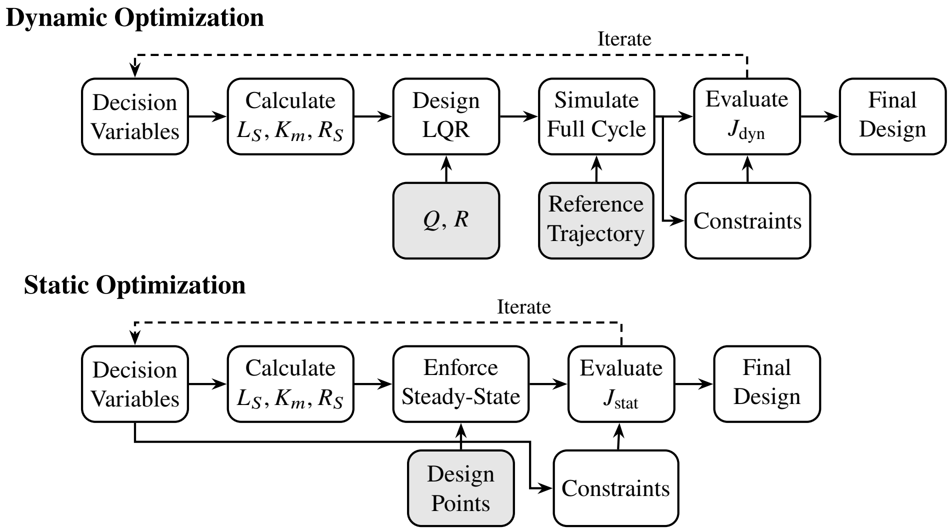


Figure 4.1 Schematic representation of the dynamic and static optimization approaches.

Table 4.2 Weights used in the cost functions and constraints.

| Weight | $w_1$ | $w_2$ | $w_3$ | $w_4$ | $w_5$ | $w_6$ | $w_7$ |
|---|---|---|---|---|---|---|---|
| Value Dynamic | 100 | $1 \cdot 10^{-3}$ | $1 \cdot 10^{6}$ | 1 | $1 \cdot 10^{3}$ | N/A | N/A |
| Value Static | N/A | $1 \cdot 10^{-3}$ | $1 \cdot 10^{3}$ | N/A | $1 \cdot 10^{5}$ | $1 \cdot 10^{10}$ | $1 \cdot 10^{5}$ |

As can be seen in Table 4.2, the weights used in the dynamic approach are different from those used in the static approach. This is due to the different nature of the two approaches, which makes it necessary to tune the weights for each approach separately. The weights were tuned, however, so that the constraints are satisfied in both approaches. It should be noted, however, that the weights were tuned using a simple heuristic approach, and no systematic exploration of the Pareto front was conducted. Thus, the results could be improved further by choosing where in the Pareto front one wants to be, and then tuning the weights accordingly, allowing for a better trade-off between the different objectives.

For the static approach, four design points were considered: maximum torque and speed; half the maximum speed and maximum torque; half the maximum torque and maximum speed point; and one that has an additional torque term to account for the acceleration, where the acceleration was chosen as the maximum acceleration in the drive cycle together with the maximum torque and speed. Those points were chosen after several attempts; they are not only somewhat representative of the drive cycle but also give the best results found in terms of the dynamical performance of the designed EMA.

The chosen drive cycle is shown as the reference position and velocity in Figure 5.1. The drive cycle emulates a simplified crane operation, where a load of $1 \cdot 10^4$ N is lifted to a height of 10 cm, held there for 1 s, and then lowered back to the initial position, where a resting time of 1 s is applied. The load is zero whenever the position is zero, simulating a load being lifted from the ground. The total duration of the drive cycle in the dynamic optimization is 5 s, although it is simulated for 11 s in all figures to show more of the performance. This drive cycle was chosen because it has a wide dynamic range, as is typical for crane applications.

For the dynamical optimization approach, the controller matrices $Q$ and $R$ were chosen as $Q = \text{diag}(5 \cdot 10^1, 5 \cdot 10^1, 1 \cdot 10^6, 1 \cdot 10^2, 1 \cdot 10^4)$ and $R = \text{diag}(1, 1)$, where diag is the diagonal matrix. Those matrices were chosen as a trade-off between performance and control effort.

# 5. Results

The optimization results shown are selected as the best design found in several attempts. The best design is chosen first by considering the constraints satisfaction, and then by the cost function value. The optimization for the dynamic approach took around 2.94 hours to complete, while the static approach took around 5.1 minutes to complete in the same machine, a standard desktop computer. At this point it must be emphasized that all the solutions found in the dynamic approach were respecting the constraints and had around the same characteristics. In contrast, in the static approach, the constraints are sometimes not satisfied and, even when they are, the characteristics of the solutions vary significantly, which makes it necessary to perform several attempts to find a good design.

The best found designs for both approaches are shown in Figure 5.1, where the position and velocity tracking are shown together.

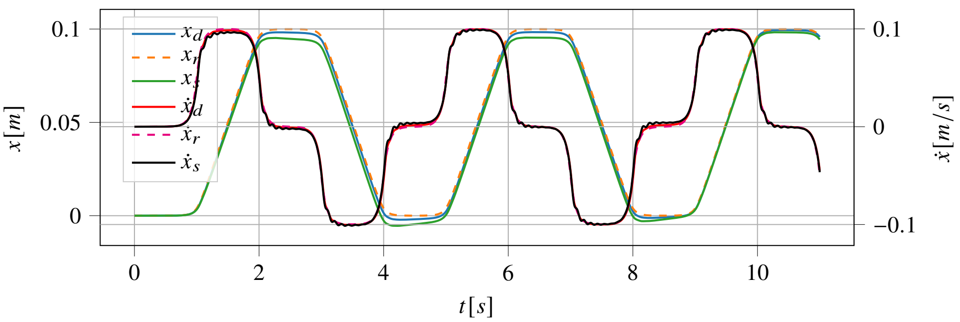


Figure 5.1 Position $x$ and velocity $\dot{x}$ tracking over the drive cycle for both optimization approaches. Within the figure, the reference trajectory is shown with subscript $r$, the designed EMA using the dynamic approach with subscript $d$ and the designed EMA using the static approach with subscript $s$.

The designed EMA using the dynamic approach was able to closely follow the desired trajectory, with very small position and velocity errors. The designed EMA using the static approach was also able to follow the desired trajectory, although not as closely. It is important to note that both designs are simulated using the same LQR controller structure with design matrices $Q$ and $R$ defined as in the dynamic optimization approach, yielding the best gain matrix $K$ for each design and allowing consistent comparison. However, it is possible to obtain better tracking performance for the static design by changing the design matrices, although this comes at the cost of increased control effort.

One very important design objective is to choose an EMA that respects the electrical constraints while being able to deliver the needed tracking performance. The current and voltage magnitudes over the drive cycle for both designs are shown in Figure 5.2, where the solid lines represent the designed EMA using the dynamic approach, while the dashed lines represent the designed EMA using the static approach.

As can be seen in Figure 5.2, the designed EMA using the dynamic approach is able to respect the electrical constraints, represented as $u_{\max}$ for the voltage and $i_{\max}$ for the current. $u_{m,d}$ hits the constraint at all points of maximum positive acceleration, while the current $i_{m,d}$ does not hit the constraint at any point. On the other hand, the designed EMA using the static approach is not close to violating any electrical constraints, but the voltage magnitude $u_{m,s}$ is very low compared to the maximum allowed voltage, at the cost of having a higher current magnitude $i_{m,s}$, not ideal for efficiency.

It is important to evaluate the efficiency of the designed EMAs over the drive cycle. The total energy losses for both designs depend on the losses in the PMSM, for which the model only considers the copper losses, and the losses in the ball screw and gears, which are the same regardless of the resulting EMA design since they were defined as having simple constant

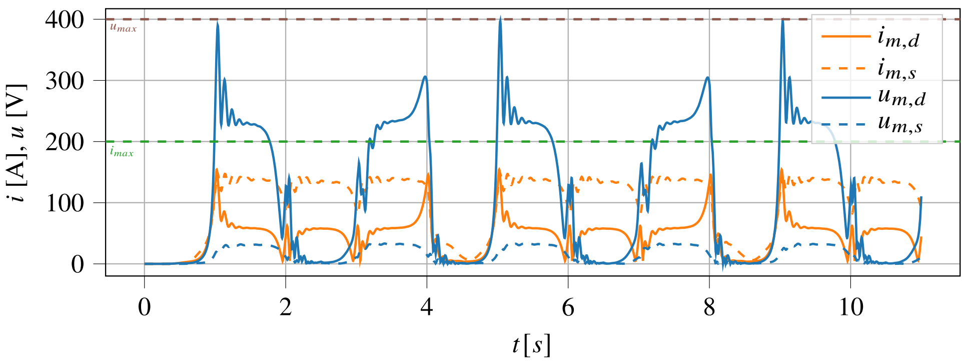


Figure 5.2 Current and voltage magnitudes over the drive cycle for both optimization approaches.

efficiencies. Thus, the only relevant comparison is the copper losses in the PMSM. The total copper losses to complete the trajectory shown in Figure 5.1 are 58 J for the dynamic design and 257 J for the static design, showing a difference in copper losses of approximately a factor of four between the two designs.

A natural question that arises is how the designed EMAs perform outside the drive cycle used in the optimization. This is reasonable to ask since the real world application is very rich in terms of possible trajectories that the EMA might need to follow. To evaluate this, both designs were simulated over a different drive cycle, one that both designs were not optimized for. The new drive cycle is shown as the reference position and velocity in Figure 5.3. This drive cycle is essentially the same as in the previous case, but with half the time to go from the initial height to the final height, thus having twice the velocity.

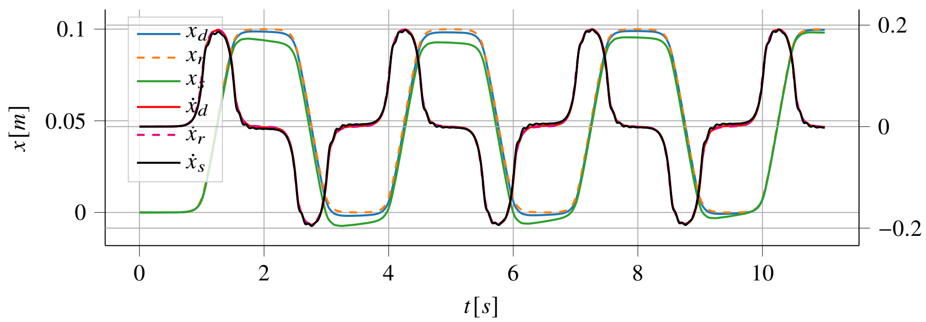


Figure 5.3 Position $x$ and velocity $\dot{x}$ tracking over a different than optimized drive cycle for both optimization approaches. Within the figure, the reference trajectory is shown with subscript $r$, the designed EMA using the dynamic approach with subscript $d$ and the designed EMA using the static approach with subscript $s$.

As can be seen in Figure 5.3, both designs have similar tracking performance over the new drive cycle, with the static design now performing even worse at tracking the reference. The currents and voltages over this new drive cycle are, as expected, higher than in the previous case, and for both designs it is exceeded at several points. One could simulate the system with restrictions on the maximum current and voltages, then, instead of the trajectory being followed at the cost of the constraints, the constraints would be kept at the cost of tracking. The former was chosen since it is much easier to implement and gives essentially the same conclusion but from a different perspective. The maximum $u_{m,d} = 1359.99$ V and $i_{m,d} = 274.09$ A for the dynamic design, while for the static design $u_{m,s} = 141.32$ V and $i_{m,s} = 197.47$ A. The total copper losses to complete this new trajectory are 131 J for the dynamic design and 261 J for the static design. Although the dynamic design became relatively worse in percentage terms, its total energy loss was much lower than that of the static design.

Another major aspect to be considered in the design of EMAs is their diameter, which was considered in the cost function. The diameter, together with the other physical decision variables of both designs, is shown in Table 5.1.

Table 5.1 Design variables of the best found designs for both optimization approaches.

| Design variable | $n_p$ | $l_2$ [m] | $l_1$ [m] | $N_S$ | $g$ [mm] | $\alpha$ [rad] | $g_{r_1}$ | $g_{r_2}$ | $p$ [mm] |
|---|---|---|---|---|---|---|---|---|---|
| Dynamic | 1 | 0.1 | 0.99 | 40 | 1.32 | 0.449 | 1.906 | 2.18 | 38.89 |
| Static | 1 | 0.103 | 0.97 | 40 | 9.47 | 1.53 | 2.36 | 4.86 | 252.23 |

Table 5.1 shows that the dynamic design has a slightly smaller diameter than the static design, at the cost of having a bigger length. This means that the dynamic design has not only better performance in terms of tracking and efficiency, but also in terms of size. It should also be noted that the dynamic design not only converged to a solution with smaller air gap $g$, but also to a solution where the operational velocity of the PMSM is much higher, a result of the different gear ratios and ball screw pitch. Both aspects are important in the design of high-performance PMSMs.

In contrast, the static design converged to a relatively large air gap, close to the upper bound of the admissible range. Since the PMSM is being optimized for efficiency, one would expect a solution closer to the minimum allowable $g$, as observed in the dynamic design. The reason for this behavior is not entirely clear, however, one possible explanation is that the static optimization problem has a larger number of local minima, increasing the likelihood that the optimizer becomes trapped in such regions.

Another important aspect of the results is that $l_1$, $l_2$, $N_S$ and $n_p$ were found by the dynamic design approach to be optimal at their bounds, showing that one could obtain better designs if the maximum number of turns and the maximum length were increased. The diameter $l_2$ was considered in the cost function directly, thus, the fact that the optimizer found the optimal value to be at the bound of $l_2$ suggests that more efficient designs could be obtained if one were to allow softer restrictions regarding the diameter or by choosing a smaller $w_2$.

## 6. Conclusions

This paper compared two preliminary EMA design strategies for a mobile machinery drive cycle: a dynamic approach that evaluates each candidate design by simulating the full trajectory with a feedback-linearized, LQR-tuned controller, and a static multi–design-point approach that enforces steady-state equations at a few representative operating points. The main finding of this work is not only to reiterate the importance of considering the entire drive cycle in the optimization problem, but also to show that it is possible to do so at a reasonable computational cost by using simplified models and efficient optimal control techniques, allowing the problem to be solved without solving the full OCP, but rather a simpler LQR problem that can be solved efficiently. As seen, although the computational cost of the dynamic approach is significantly higher for one optimization round, the static approach required several attempts to find a marginally acceptable design, making the dynamic approach more efficient in practice.

As discussed, the designs in Table 5.1 are not valid for the actual design of real EMAs, since the model purposely neglects several important aspects that are usually the limiting factors, such as thermal limits, saturation effects and more complete loss models. Moreover, the considered drive cycle is oversimplified and choosing a representative one was not addressed. The main goal of this work is, however, to show the potential of considering the entire drive cycle in the optimization problem without neglecting the dynamics of the EMA, a picture that was clearly shown by the results, where every designed aspect considered was significantly better for the dynamic approach.

The significantly lower losses of the dynamic approach result from the model considering only copper losses: by respecting electrical constraints while tracking trajectories, it finds designs that require lower currents. While more complete models with iron losses would reduce the relative loss difference between approaches, the dynamic approach is expected to remain superior due to its consideration of full EMA dynamics over the drive cycle.

## 7. FUTURE WORK

Future work should address four main areas: incorporating more complete EMA models including thermal limits, saturation effects, and iron losses to enable realistic preliminary designs; validating the simplified optimization-oriented models; comparing the LQR-based control approach against full OCP solutions to assess the optimality gap in this system; and the pareto front of the different designs, that is, how the different weights in the cost function affect the resulting design. This would allow for a better understanding of the trade-offs involved in the design of EMAs for mobile machinery applications. Those improvements would allow much better preliminary design of EMAs, reducing the number of refinements needed using more complete finite element models.

## REFERENCES

[1] A. Rankka, A. Dell'Amico, and P. Krus, 'Drive cycle generation for a hydraulic loader crane', in The Sixteenth Scandinavian International Conference on Fluid Power, May 22-24, 2019, Tampere, Finland, Tampere University of Technology, 2019, pp. 42–53.

[2] O. Borsboom, M. Salazar, and T. Hofman, 'Electric Motor Design Optimization:A Convex Surrogate Modeling Approach', en, IFAC-PapersOnLine, vol. 55, no. 24, pp. 373–378, 2022, ISSN: 24058963. DOI: 10.1016/j.ifacol.2022.10.312.

[3] S. Pastellides, S. Gerber, R.-J. Wang, and M. Kamper, 'Evaluation of Drive Cycle-Based Traction Motor Design Strategies Using Gradient Optimisation', en, Energies, vol. 15, no. 3, p. 1095, Jan. 2022, Number: 3 Publisher: Multidisciplinary Digital Publishing Institute, ISSN: 1996-1073. DOI: 10.3390/en15031095.

[4] E. Roshandel, A. Mahmoudi, W. Soong, and S. Kahourzade, 'Optimal Design of Induction Motors Over Driving Cycles for Electric Vehicles', IEEE Transactions on Vehicular Technology, pp. 1–15, Jul. 2023. DOI: 10.1109/TVT.2023.3292901.

[5] A. E. Bryson, 'Applied Optimal Control: Optimization, Estimation and Control'. New York: Routledge, May 2018, ISBN: 978-1-315-13766-7. DOI: 10.1201/9781315137667.

[6] F. L. Lewis, D. Vrabie, and V. L. Syrmos, 'Optimal Control', English. Hoboken: Wiley, 2012, ISBN: 978-0-470-63349-6.

[7] B. Colson, P. Marcotte, and G. Savard, 'An overview of bilevel optimization', en, Annals of Operations Research, vol. 153, no. 1, pp. 235–256, Sep. 2007, ISSN: 1572-9338. DOI: 10.1007/s10479-007-0176-2.

[8] J. Chiasson, 'Modeling and High Performance Control of Electric Machines', en. John Wiley & Sons, May 2005, Google-Books-ID: cq6RPPsOyt8C, ISBN: 978-0-471-72234-2.

[9] 'Solve_continuous_are — SciPy v1.16.2 Manual'.

[10] 'Differential_evolution — SciPy v1.16.2 Manual'.

[11] M. Wormington, C. Panaccione, K. M. Matney, and D. K. Bowen, 'Characterization of Structures from X-Ray Scattering Data Using Genetic Algorithms', Philosophical Transactions: Mathematical, Physical and Engineering Sciences, vol. 357, no. 1761, pp. 2827–2848, 1999, Publisher: The Royal Society, ISSN: 1364-503X.

[12] J. Qiang and C. Mitchell, 'A Unified Differential Evolution Algorithm for Global Optimization', IEEE Transactions on Evolutionary Computation, Jun. 2014.

## Biographies

**Róger Mateus Sehnem**. He received his Bachelor in Aerospace Engineering (UFSM) in 2021 and his M.Sc in Electrical Engineering (UFRGS) with emphasis on data driven control in 2023. He currently works as a PhD student with electromechanical actuators with focus on dynamics, control and optimization. His research interests include control, system modelling, optimal control, machine learning, and optimization.

**Samuel Kärnell**. He received his Ph.D. in Hydraulics at Linköping University (LiU), Sweden, in 2022. He currently works as a Assistant Professor at Fluid and Mechatronic Systems at LiU. His research interests include pump and motor design, electro-hydraulic systems, electrification of mobile machinery, and karaoke.

**Liselott Ericson**. She received her Ph.D. in Hydraulics at Linköping University (LiU), Sweden, in 2012. She currently works as a professor at Fluid and Mechatronic Systems at LiU. Her research interests include pump and motor design, electro-hydraulic systems, modelling and simulation, and optimisation.